Publication P4

Seman, S., Niiranen, J., Kanerva, S., Arkkio, A., Saitz, J. 2005. “Performance Study of Doubly Fed Wind-Power Generator under Network Disturbances”, *IEEE Transaction on Energy Conversion*, Accepted for future publication, 8 p., Available: http://ieeexplore.ieee.org/iel5/60/26781/101109TEC2005853741.pdf?tp=&arnumber=101109TEC2005853741&isnumber=26781, (7.5.2006).

Performance Study of a Doubly Fed Wind-Power Induction Generator under Network Disturbances

Slavamir Seman, *Student Member, IEEE*, Jouko Niiranen, *Senior Member, IEEE*, Sami Kanerva, Antero Arkkio, and Julius Saitz

***Abstract*—Transient performance of a 1.7-MW wind-power doubly fed induction generator (DFIG) under network disturbances is studied using a coupled field-circuit simulator. The simulator consists of the finite-element method model of a DFIG coupled with the circuit model of the frequency converter, a transformer, and a simple model of the network. The simulation results show the transient behavior of the DFIG when a sudden voltage dip is introduced. The field-circuit simulator is experimentally validated by full-power measurement.**

***Index Terms*—Coupled model, crowbar, doubly fed induction generator (DFIG), finite-element method (FEM), measurement, voltage dip.**

I. Introduction

In THE recent years, the number of variable-speed wind turbines with doubly fed induction generators (DFIGs) connected to the national networks has increased. This is mainly due to their ability to supply power at constant voltage and frequency while the rotor speed varies, which allows a better wind capture in comparison with fixed-speed wind turbines.

Due to penetration of variable-speed wind turbines with DFIG into the national grids, utilities ask for an active control of the wind-turbines during network disturbances. According to proposals of the new network codes, a wind generator should stay connected to the network for prescribed time interval that depends on voltage dip level [1]. This requirement needs to be taken into account in wind turbine designing process.

The designing process of a new generation wind turbine with ride-through capability requires new simulation tools that help explain the impact of the power system disturbances on a wind turbine operation.

Analyses of DFIG systems presented in literature in the recent years were performed on several levels. An analytical transient model of a doubly fed induction machine and its experimental validation is presented in [2]. The finite-element method (FEM)-based approach was used for analysis of a 100 kW brushless doubly fed induction generator [3]. The simulated torque—speed characteristic was compared with measurement.

Manuscript received November 18, 2004; revised March 17, 2005. This work was supported in part by The National Technology Agency of Finland, ABB Oy Fortum Oyj and the Fortum Foundation. Paper no. TEC-00329-2004.

S. Seman, and A. Arkkio are with the Laboratory of Electromechanics, Helsinki University of Technology, Helsinki, FIN-02015 HUT, Finland (e-mail: slavomir.seman@hut.fi; antero.arkkio@hut.fi).

J. Niiranen and S. Kanerva, are with ABB Oy, Helsinki, FIN-00381, Finland (e-mail: jouko.niiranen@fi.abb.com; sami.kanerva@fi.abb.com).

J. Saitz is with Ansoft Corporation, 225 West Station Square Drive, Pittsburgh, PA 15219, USA (e-mail: jsaitz@ansoft.com).

Digital Object Identifier 10.1109/TEC.2005.853741

Transient studies focused on power system stability and power quality investigation as well as grid integration of DFIG wind turbines that use more or less complex shaft system models and analytical equivalent-circuit—based models of a generator, usually of reduced order [4]–[6].

Detailed simulation transient analysis of a 2-MW wind-power DFIG including a model of control and crowbar protection under grid disturbances is presented in [7]. A three-phase analytical model of a 1.75-MW DFIG for transient stability studies was presented and benchmarked with advanced model in [8]. Transient behavior of a DFIG wind turbine was studied in [9], comparing simulations with measurements on a 22-kW laboratory test setup. Dynamic behavior of a 660-kW DFIG wind turbine was studied and validated by measurements in [10].

In most of the above-mentioned papers, only analytical models of DFIG are used that do not represent the variation of the equivalent circuit parameters due to magnetic saturation. The simulation results in [11] show that magnetic saturation needs to be taken into account in order to get more accurate results.

This paper presents a performance study of a 1.7-MW wind-power DFIG under grid disturbance. The simulation scheme consists of either an FEM or analytical model of DFIG, whereas the frequency converter, transformer, network, and control parts are modeled in a system simulator. The simulator also includes a detailed model of a frequency converter that is controlled by a modified direct torque control (DTC) strategy.

The simulation results were verified by a full-scale measurement setup. The setup consisted of a wind-power DFIG and a frequency converter that are used for variable speed 2-MW wind turbines, a large synchronous generator acting as a grid, and two transformers. The generator was powered by a prime mover at constant speed instead of the 2-MW wind turbine. These tests were performed in laboratory, as it was not possible to make field tests on a 2-MW wind turbine during the grid fault.

II. Method of Experiment

A. Description of the Test Setup

A single line diagram of a full-scale measurement setup is shown in Fig. 1 and its photograph in Fig. 2. DFIG with a stator current rating of 1600 A can be loaded to generate more than 2 MW when run in the maximum super-synchronous speed. The transformer TR 1 transforms the synchronous generator output voltage 11.5 kV to the 690 V that is the voltage level of the doubly fed equipment. The other transformer TR 2 is used as short circuit impedance.

The test is started with both the transformers connected, that is, circuit breaker SW2 is closed and SW1 is open. Closing the

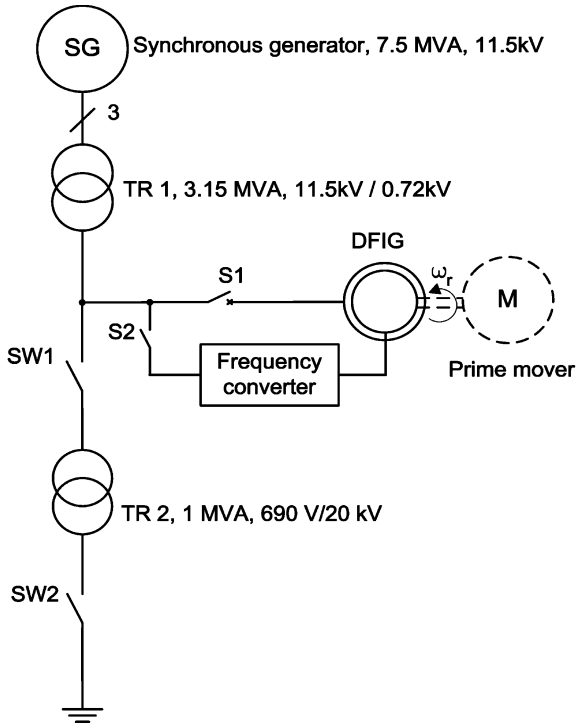

Fig. 1. Schematic diagram of the test setup.

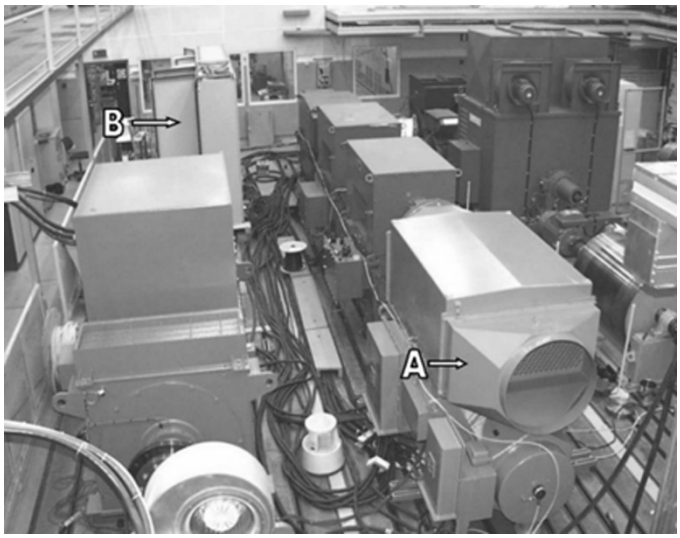

Fig. 2. Photograph of a part of the test setup at ABB test laboratory. DFIG is marked with "A" on the right. The frequency converter is a cabinet marked with "B" on the left.

circuit breaker SW1 in the transformer's secondary generates the voltage dip and opening the circuit breaker SW2 terminates the voltage dip.

B. Frequency Converter Operation

The rotor of DFIG is supplied from the frequency converter that consists of a back-to-back connected network-side converter and a rotor-side converter equipped with passive crowbar [12] as it is depicted in Fig. 3.

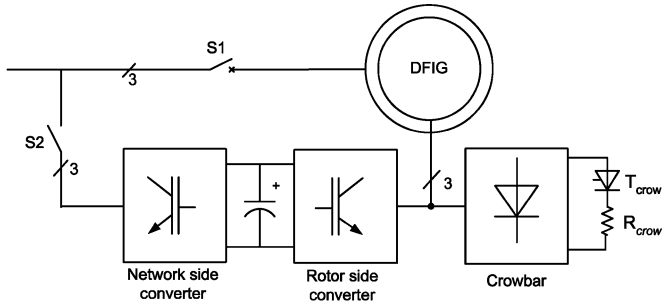

Fig. 3. Frequency converter equipped with crowbar.

1) Network-Side Converter: The aim of the control of the network-side converter is to maintain the level of dc-link voltage $U_{\rm dc}$ on a pre-set value. $U_{\rm dc}$ is controlled by a PI controller—based algorithm.

2) Rotor-Side Converter Control: The rotor-side converter is in fact a voltage source inverter that is controlled by a modified DTC strategy [13].

In the conventional DTC, the torque controller determinates the switching instances of the inverter in order to control the induction machine torque. However, the modified torque controller controls the desired amount of the generated electric power and power factor. The torque controller also performs the "line synchronization" so that the generator can be smoothly connected to and disconnected from the grid.

The frequency converter operates if the rotor speed is in the range of 70%–130% of the rated synchronous speed. The switch S2 is closed in order to start the operation of the network-side converter and establish the dc-link voltage. At the same time the rotor-side converter measures the grid and stator voltage and starts the line synchronization.

After synchronization the main circuit breaker S1 connects the stator of the generator to the grid and the control of the rotor-side converter is switched to torque-control mode with a power factor demand defined by the user.

The shutdown of the system is performed so that first the torque reference is set to zero and the power factor demand is set to 1. The stator current should be about zero. The main circuit breaker S1 is opened and both the rotor-side and network-side converters are switched off.

3) Rotor Over-Current Protection: The rotor over-current protection (passive crowbar) eliminates high rotor currents during power system disturbances when the generator is connected to the grid. The passive crowbar circuit depicted in Fig. 3 consists of a three-phase diode bridge that rectifies the rotor currents and a single thyristor $T_{\rm crow}$ in series with a resistor $R_{\rm crow}$.

When the network disturbance is introduced, high currents are induced to the rotor from the stator side. This also causes a rapid increase of a dc-link voltage and a dc-link over-voltage protection will send the command to the torque control to stop modulation and turn on the crowbar control thyristor. The rotor is now connected to the crowbar and remains connected until the main circuit breaker disconnects the stator from the grid. After clearance of the fault the generator can be line-synchronized again and started in a normal operation mode.

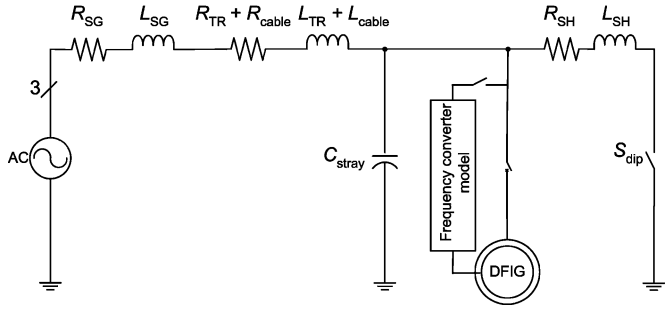

Fig. 4. Circuit model of the test setup.

III. Method of Analysis

The experimental setup presented in the previous section was modeled by means of a coupled circuit—field simulator that consists of a circuit-based model of the test set-up and an FEM model of the studied DFIG. A "T" equivalent circuit-based model of the DFIG with constant lumped parameters was also implemented into the simulator and benchmarked with the FEM model.

A. Model of the Test Setup

The model of the test setup network used in simulation is depicted in Fig. 4. The scheme consists of a three-phase voltage source model in series with a short circuit inductance L_{SG} and resistance R_{SG} that represent a simple model of the synchronous generator SG. The time variation of the SG voltage amplitude and frequency was defined in the simulator by lookup table data that were extracted from the measured voltage.

A transmission line between the network and the transformer is modeled with its resistance R_{cable} and inductance L_{cable}. The main transformer is represented by a simple linear model, i.e., magnetic saturation was not taken into account. The transformer model contains a short circuit resistance R_{TR}, inductance L_{TR} and stray capacitance of the winding C_{stray}.

The transformer that generates the voltage dip by closing the switch $\mathrm{S_{dip}}$ is represented by its short circuit resistance R_{SH} and inductance L_{SH}.

B. Modeling of the Frequency Converter

The network-side converter is modeled by a transfer function of the first order discrete filter. The control of the dc-link voltage level is realized by a PI controller-based algorithm.

The model of the rotor-side DTC controlled converter is rather complex. The control algorithms, flux estimators, and reference value calculators, together with the switching lookup table are implemented by dynamically linked code (S-function) into Matlab-Simulink and coupled with other parts of the simulator [14]. The voltage source inverter is modeled as a three-phase bridge with 3 positive and 3 negative ideal switches. The switches are controlled by switching instances generated by DTC control. The output voltages of the voltage inverter model supply the rotor circuit of the DFIG model.

The operation of the crowbar was represented by an algorithm that deactivates the rotor side converter upon the detection of the over-voltage in a dc-link. The rotor is then connected to the three-phase diode bridge with the resistance connected in parallel by turning on the ideal switch which represents the control crowbar thyristor.

C. Equivalent-Circuit-Based Analytical Model of the DFIG

The machine equations written in an x–y reference frame fixed to the rotor are

$$\frac{\mathrm{d}\psi_{\mathrm{s\_x}}}{\mathrm{d}t} = \sigma_{\mathrm{S}}\left(\frac{L_{\mathrm{r}}}{L_{\mathrm{m}}}\psi_{\mathrm{s\_x}} - \psi_{\mathrm{r\_x}}\right) - p\omega_{\mathrm{r}}\psi_{\mathrm{s\_x}} + v_{\mathrm{s\_y}} \quad (1)$$

$$\frac{\mathrm{d}\psi_{\mathrm{s\_y}}}{\mathrm{d}t} = \sigma_{\mathrm{S}}\left(\frac{L_{\mathrm{r}}}{L_{\mathrm{m}}}\psi_{\mathrm{s\_y}} - \psi_{\mathrm{r\_y}}\right) - p\omega_{\mathrm{r}}\psi_{\mathrm{s\_y}} + v_{\mathrm{s\_x}} \quad (2)$$

$$\frac{\mathrm{d}\psi_{\mathrm{r\_x}}}{\mathrm{d}t} = \sigma_{\mathrm{R}}\left(\psi_{\mathrm{r\_x}} - \frac{L_{\mathrm{m}}}{L_{\mathrm{s}}}\psi_{\mathrm{s\_x}}\right) + v_{\mathrm{r\_x}} \quad (3)$$

$$\frac{\mathrm{d}\psi_{\mathrm{r\_y}}}{\mathrm{d}t} = \sigma_{\mathrm{R}}\left(\psi_{\mathrm{r\_y}} - \frac{L_{\mathrm{m}}}{L_{\mathrm{s}}}\psi_{\mathrm{s\_y}}\right) + v_{\mathrm{r\_y}}, \quad (4)$$

where

$$\sigma_{\mathrm{S}} = \frac{R_{\mathrm{s}}L_{\mathrm{m}}}{L_{\mathrm{m}}L_{\mathrm{m}} - L_{\mathrm{s}}L_{\mathrm{r}}}$$

$$\sigma_{\mathrm{R}} = \frac{R_{\mathrm{r}}L_{\mathrm{s}}}{L_{\mathrm{m}}L_{\mathrm{m}} - L_{\mathrm{s}}L_{\mathrm{r}}}$$

$$i_{\mathrm{s\_x}} = \frac{L_{\mathrm{m}}}{L_{\mathrm{m}}L_{\mathrm{m}} - L_{\mathrm{s}}L_{\mathrm{r}}}\left(\psi_{\mathrm{r\_x}} - \frac{L_{\mathrm{r}}}{L_{\mathrm{m}}}\psi_{\mathrm{s\_x}}\right) \quad (5)$$

$$i_{\mathrm{s\_y}} = \frac{L_{\mathrm{m}}}{L_{\mathrm{m}}L_{\mathrm{m}} - L_{\mathrm{s}}L_{\mathrm{r}}}\left(\psi_{\mathrm{r\_y}} - \frac{L_{\mathrm{r}}}{L_{\mathrm{m}}}\psi_{\mathrm{s\_y}}\right) \quad (6)$$

$$i_{\mathrm{r\_x}} = \frac{L_{\mathrm{s}}}{L_{\mathrm{m}}L_{\mathrm{m}} - L_{\mathrm{s}}L_{\mathrm{r}}}\left(\frac{L_{\mathrm{m}}}{L_{\mathrm{s}}}\psi_{\mathrm{s\_x}} - \psi_{\mathrm{r\_x}}\right) \quad (7)$$

$$i_{\mathrm{r\_y}} = \frac{L_{\mathrm{s}}}{L_{\mathrm{m}}L_{\mathrm{m}} - L_{\mathrm{s}}L_{\mathrm{r}}}\left(\frac{L_{\mathrm{m}}}{L_{\mathrm{s}}}\psi_{\mathrm{s\_y}} - \psi_{\mathrm{r\_y}}\right) \quad (8)$$

$$T_{\mathrm{e}} = \frac{3}{2}p\left(\psi_{\mathrm{s\_y}}i_{\mathrm{s\_x}} - \psi_{\mathrm{s\_x}}i_{\mathrm{s\_y}}\right). \quad (9)$$

The symbols i_{s} and i_{r} denote the stator and rotor currents, respectively, v_{s} and v_{r} denote stator and rotor voltages and ψ_{s} and ψ_{r} stator and rotor flux linkages in two axis rotational (x–y) reference frames. R_{s} and R_{r} are stator and rotor resistance and $L_{s,}L_{\mathrm{r}},$ and L_{m} are stator, rotor, and magnetizing inductance, respectively. The rotor speed is denoted as ω_{r}. Symbol p represents the number of pole-pairs, and T_{e} is the electromagnetic torque. The equation of the movement is omitted and the rotor speed is considered to be constant.

D. Finite Element Model of DFIG

The magnetic field in the generator is modeled by two-dimensional finite element analysis and coupled with the voltage equations of the windings [15]. The z-component of the magnetic vector potential A satisfies

$$\nabla\cdot(\nu\nabla A) - \sigma\frac{\mathrm{d}}{\mathrm{d}t}A + \frac{Ni_{\mathrm{w}}}{S_{\mathrm{w}}} = 0 \quad (10)$$

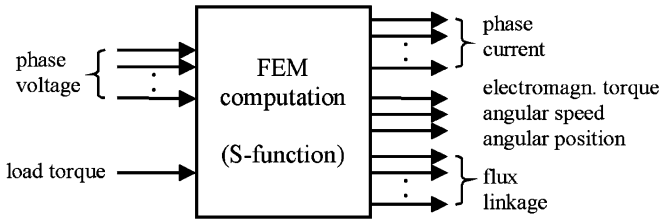

Fig. 5. Functional block of the FEM computation.

where ν is the nonlinear reluctivity, σ is the conductivity, and N is the number of turns in the coil with a cross section area S_{w} and carrying the phase current i_{w}. Since there are no damping bars in the rotor and the conductivity in the laminated iron core is set to zero, the derivative term in (10) only covers the effect of eddy currents in the steel shaft. The voltage equations for the windings are in the form

$$u_{\mathrm{w}} = \sum_{k=1}^{n_{\mathrm{c}}} \beta_k l_k \frac{\mathrm{d}}{\mathrm{d}t} A_k^{\mathrm{ave}} + R i_{\mathrm{w}} + L_{\mathrm{e}} \frac{\mathrm{d}}{\mathrm{d}t} i_{\mathrm{w}} \qquad (11)$$

where u_{w} is the phase voltage, n_{c} is the total number of coil sides in the winding, β_k is either a positive or negative multiplier according to the orientation of the coil side, l_k is the length of the coil side, A_k^{ave} is the average vector potential on the coil side, R is the total resistance of the coil, and L_{e} is the additional end-winding inductance.

The electromagnetic torque T_{e} is determined from the field solution using the virtual work principle

$$T_{\mathrm{e}} = \frac{\mathrm{d}}{\mathrm{d}\theta} \int_{\Omega} \int_{0}^{H} B \cdot \mathrm{d}H \mathrm{d}\Omega \qquad (12)$$

where θ is the position angle of the rotor and Ω is the cross section of the air gap. The magnetic flux density B and the magnetic field strength H are determined from the field solution. The angular frequency of the rotor can be considered constant or solved by the equations of motion.

The FEM computation is implemented as a functional block in Matlab-Simulink using dynamically linked program code (S-function). Voltages of the phase windings in stator and rotor are given as input variables and the phase currents, electromagnetic torque, rotational speed, rotor position, and flux linkages in stator and rotor are obtained as output variables, as illustrated in Fig. 5.

In time-stepping simulation, the FEM computation is coupled with Matlab-Simulink by an indirect procedure [16]. This means that the time-stepping FEM computation runs at major time steps, which are usually longer than the minor steps elsewhere in the system model in Simulink. Accordingly, the output variables from FEM computation are kept constant during a period of several minor steps in the total system model, and changes in the variables take effect at major steps.

In spite of the indirect coupling, the accuracy of the results can be maintained by choosing the major and minor time steps appropriately according to the physical time constants. In addition, shortening the steps in the converter model with respect to the FEM model can reduce time consumption of the simulation, because the time-consuming FEM solution is not determined too frequently.

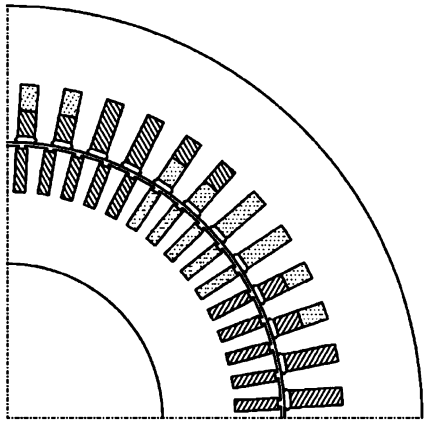

Fig. 6. Geometry of the DFIG model.

TABLE I
PARAMETERS OF THE DFIG

P_{N}	rated power	1.7 MW
U_{N}	rated stator voltage	690 V (delta)
I_{N}	rated stator current	1600 A
$U_{\mathrm{max,r}}$	maximum rotor voltage [1]	2472 V (star)
f_{N}	rated stator frequency	50 Hz
n_{N}	nominal speed	1500 rpm

[1] In normal use the rotor voltage is proportional to slip

The finite element mesh of the DFIG covers one quarter of the cross section, comprising 949 nodes and 1848 linear triangular elements. The geometry of the model is presented in Fig. 6, and the parameters of the DFIG are presented in Table I.

IV. Results and Discussion

The simulation analysis was carried out in a Matlab-Simulink system simulator. The system simulator was running with the time step $\mathrm{T_{step}} = 0.5 \cdot 10^{-7}$ s and Forward Euler method has been used. The FEM model of DFIG was running with the time step $\mathrm{T_{stepFEM}} = 0.5 \cdot 10^{-4}$ s. In the first sequence of the simulation, the generator is synchronized with the network and after 2.5 s the rotor—side converter starts to control DFIG in torque control mode by setting a constant reference torque to value $T_{\mathrm{ref}} = -9.826$ kN at constant speed $\omega_{\mathrm{r}} = 1760$ r/min.

The demanded value of the power factor is set to 1, and the maximum value of the dc-link voltage to 1050 V.

The network disturbance is introduced at 5.0037 s, when the stator voltage decreases. At the time instance of 5.12 s, the generator is disconnected from the network by opening the main circuit breaker and the frequency converter is shut down.

Fig. 7. depicts the stator phase voltage. When the short circuit is introduced the amplitude of the voltage drops down to 35% and continues its decrease to 20% of the nominal value. A small increase of frequency can be observed as well. This is because the synchronous generator in an experimental setup is not a rigid enough power source and the SG excitation controller is not fast enough.

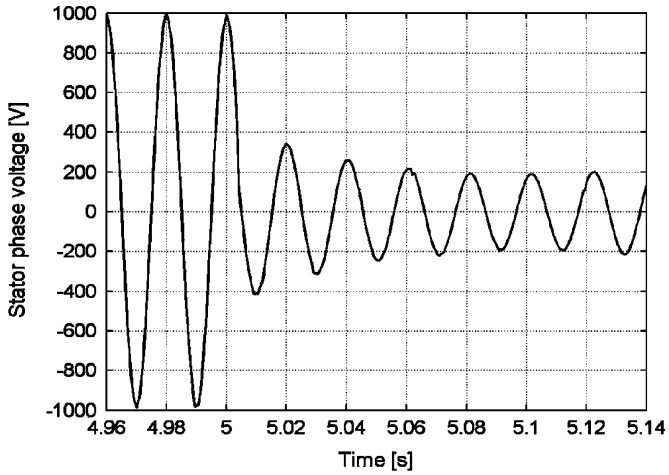

Fig. 7. Stator phase voltage during the grid disturbance.

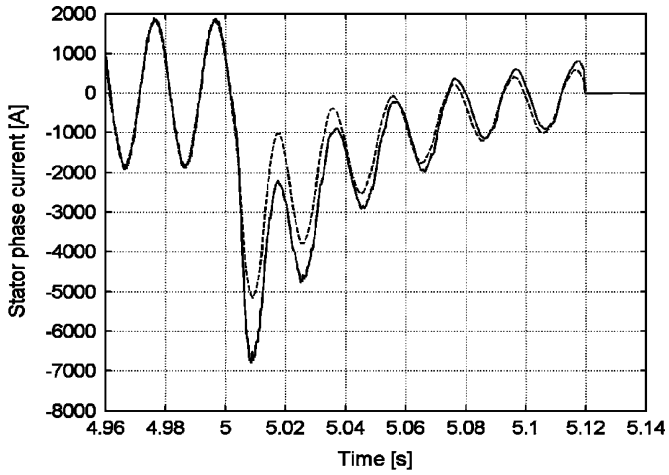

Fig. 9. Transient stator current obtained from FEM model (solid) and transient stator current obtained by analytical model (dashed).

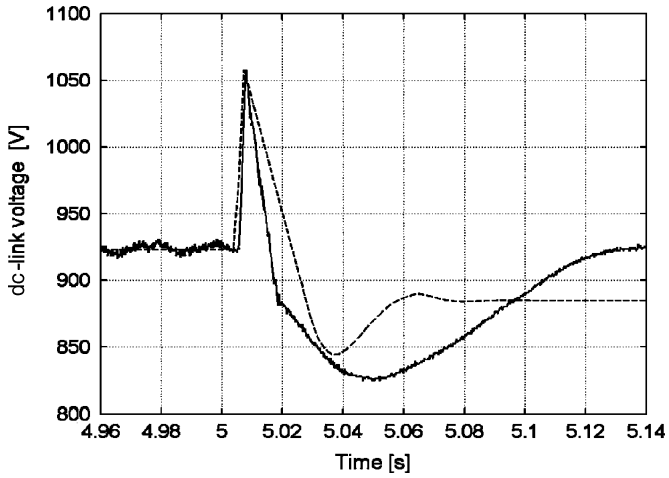

Fig. 8. Comparison of the simulated (dashed) and measured (solid) dc-link voltage waveform during the grid disturbance.

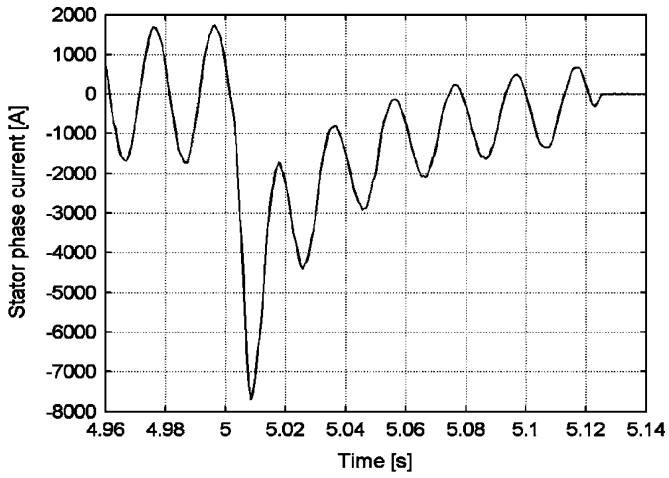

Fig. 10. Measured transient stator current.

The comparison of the measured and simulated dc-link voltages is shown in Fig. 8. During the transient both the voltages rise up to a maximum value of about 1050 V almost at the same time instant. After the dc-link voltage level reaches its maximum, the over-voltage protection stops the modulation of the rotor-side converter and disconnects the rotor from the dc-link. The dc-link voltage starts to decrease and after a while reaches a new steady state value. The measured dc-link voltage settles much slower than the simulated one. This is because the network-side converter is modeled as a simple first order filter transfer function and the dc-link voltage controller is represented by a simple PI controller, whereas the real network-side converter is a converter with complex control.

Fig. 9. shows the comparison of the simulated transient stator current obtained by FEM model and analytical model. At the beginning of the transient, a significant difference in amplitude can be observed between the stator FEM current and the stator current from analytical model. The difference is decreasing and after 5.06 s both the waveforms show good agreement. The difference in the amplitude during the first period of the transient current is mainly due to neglecting the magnetic saturation in the analytical model.

The measured transient stator current is shown in Fig. 10. The waveform of the transient current corresponds well with both the (FEM and analytical) simulated ones. The amplitude of the measured transient current is higher during the first period than the current amplitude calculated by FEM and the difference is about 1 kA. The difference between the measured transient current and the current obtained by the analytical model in the beginning of the transient is about 2.6 kA. In the time interval of 5.04–5.08 s, the compared currents are in good agreement. The simulated currents slightly differ from the measured current during the last two periods. A possible reason for that is inaccuracy of the test setup model parameters.

Fig. 11 depicts the time variations of the transient rotor current calculated by means of the analytical model and the transient rotor current obtained from FEM model of DFIG. The comparison shows the difference between the simulated currents in the beginning of the transient. The amplitude of the rotor current calculated by FEM is in the first half period higher than the transient rotor current calculated by the analytical model and

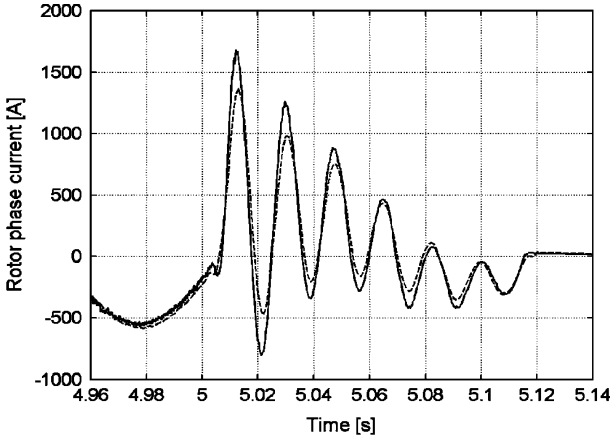

Fig. 11. Transient rotor current obtained form FEM model (solid) and transient rotor current obtained by analytical model (dashed).

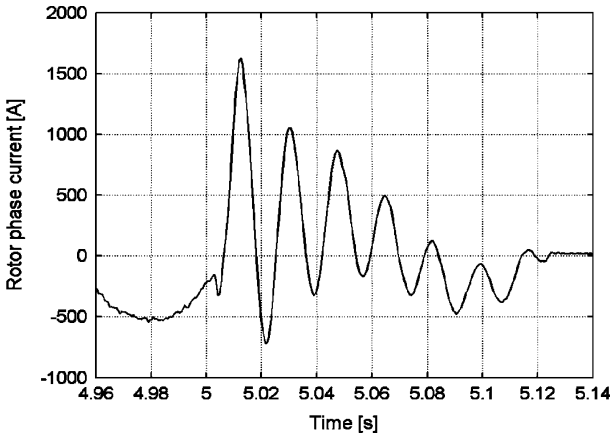

Fig. 12. Measured transient rotor current.

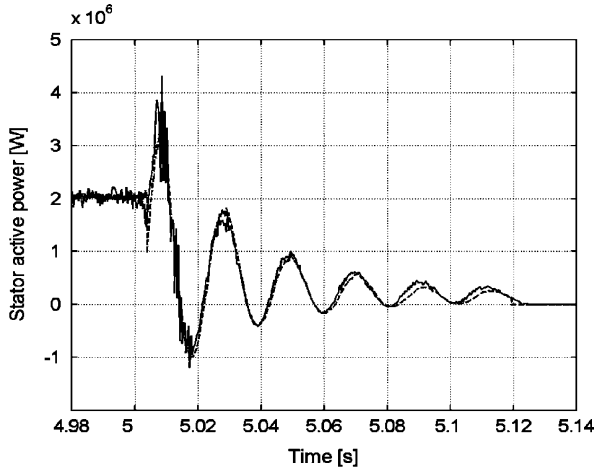

Fig. 13. Comparison of the stator active power calculated from measured values (solid) and from simulated (FEM) values (dashed).

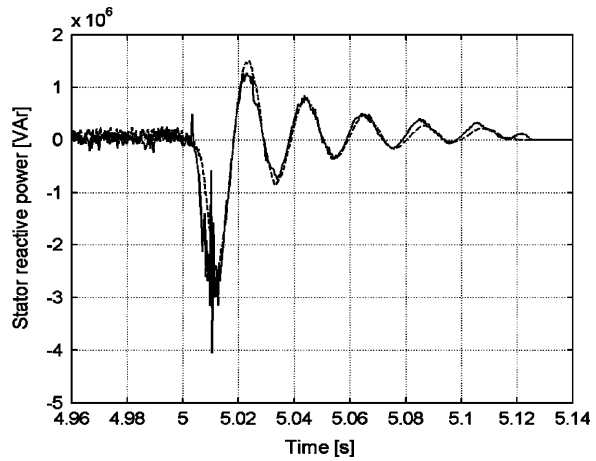

Fig. 14. Comparison of the stator reactive power calculated from measured values (solid) and from simulated (FEM) values (dashed).

the difference is about 400 A. The difference in amplitude decreases slowly and after the time instance of 5.1 s, both curves are in good agreement.

Fig. 12 shows the measured phase rotor current of DFIG after grid disturbance. During the first period the amplitude of the measured transient rotor current equals to the current amplitude calculated by FEM. The amplitude of the transient rotor current obtained by the analytical model is lower by 400 A than the amplitude of the measured rotor current. The difference between the simulated and measured waveforms can be observed after the time instant of 5.05 s probably due to inaccuracy of the test setup equivalent circuit parameters.

Figs. 13 and 14 show the stator instantaneous active power $P_{\rm inst}$ and reactive power $Q_{\rm inst}$, respectively. The powers are determined using the simulated (FEM) and measured values of the current and voltage according to the following:

$$P_{\rm inst} = \frac{3}{2}(v_{\rm s\_d} i_{\rm s\_d} + v_{\rm s\_q} i_{\rm s\_q}) \tag{13}$$

$$\mathrm{Q}_{\rm inst} = \frac{3}{2}(v_{\rm s\_d} i_{\rm s\_q} - v_{\rm s\_q} i_{\rm s\_d}). \tag{14}$$

Here, the symbols $i_{\rm s}$ and $v_{\rm s}$ denote the stator currents and voltages and index d denotes the real and q the imaginary part of the stator voltage and current space vector.

The active and reactive powers reconstructed from the simulation results show good agreement with the curves calculated from the measurements except at the beginning of the transients where the power obtained from the measured values is higher and the difference is about 15% in the first peak value and about 10% in second peak. The analytical and the FEM simulation results are almost identical, and their comparison was omitted. The comparison of the active and reactive power curves during the transient calculated from FEM simulation results and measurements shows only a little difference.

The FEM simulation results agree with the measured results better than the analytical simulation results. This is mainly because of the stator and rotor leakage inductance variation caused by magnetic saturation that is taken into account in FEM, whereas in the analytical model the lumped parameters are considered to be constant. In a transient performance simulation study it is important to use a FEM model of the generator

or a model which takes into account the magnetic saturation that will give a significantly more realistic view of the maximum currents in the stator and rotor during a grid disturbance than the analytical model. This is important, especially, for dimensioning of the power electronics and for development and optimization of the wind-power generators. However, it is sometimes enough to use a simulator based on an analytical model for a power system transient stability analysis during a symmetrical grid fault. This is not so time consuming as using an FEM model.

V. Conclusion

The transient behavior of a doubly fed wind-power induction generator connected to the grid and controlled by modified direct torque control during a power system disturbance was studied. The coupled field-circuit model based simulator has been used and compared with the analytical model based simulator. The full-power transient measurements on the test setup with a 1.7-MW doubly fed wind-power generator were carried out in order to verify the simulation results.

The comparison between the simulated and measured results shows a reasonable agreement. The analytical model of DFIG manifests certain drawbacks that are overcome by using a FEM model. The developed coupled field-circuit based simulator has proved to be capable and reliable for modeling complicated power electronics and electric machine setups and thus a useful tool for the development and optimization of the wind-power generators.

Appendix

A. *DFIG equivalent circuit parameters*
Star equivalent circuit parameters
- resistances at 20 °C temperature
- reactances at 50-Hz frequency

$R_{\mathrm{s}} = 1.615\ \mathrm{m\Omega}$
$X_{\mathrm{s}\sigma} = 28.83\ \mathrm{m\Omega}$
$X_{\mathrm{m}} = 787.8\ \mathrm{m\Omega}$
$R'_{\mathrm{r}} = 2.369\ \mathrm{m\Omega}$
$X'_{\mathrm{r}\sigma} = 25.77\ \mathrm{m\Omega}.$

B. TR 1 *equivalent circuit parameters*
$X_{\mathrm{TR}} = 9.07\ \mathrm{m\Omega}$
$R_{\mathrm{TR}} = 1.51\ \mathrm{m\Omega}.$
TR 2 *equivalent circuit parameters*
$X_{\mathrm{SH}} = 29.5\ \mathrm{m\Omega}$
$R_{\mathrm{SH}} = 4.76\ \mathrm{m\Omega}.$

C. *Parameters of a synchronous generator equivalent L-R model based on the transient impedance*
$X_{\mathrm{SG}} = 20.8\ \mathrm{m\Omega}$
$R_{\mathrm{SG}} = 0.527\ \mathrm{m\Omega}.$

D. *Parameters of 100 meters of 690-V cable equivalent L-R model.*
$X_{\mathrm{cable}} = 11\ \mathrm{m\Omega}$
$R_{\mathrm{cable}} = 15\ \mathrm{m\Omega}.$

References

[1] E. ON Netz Gmbh, Germany. (2003, Aug.). Grid code for high and extra highvoltage. [Online]. Available: http://www.eonnetz.com/Ressources/downloads/enenarhseng1.pdf

[2] M. S. Vicatos and J. A. Tegopoulos, "Transient state analysis of a doubly-fed induction generator under three phase short circuit," *IEEE Trans. Energy Convers.*, vol. 6, no. 1, pp. 62–68, Mar. 1991.

[3] F. Runcos, R. Carlson, A. M. Oliveira, P. Kuo-Peng, and N. Sadowski, "Performance analysis of a brushless double fed cage induction generator," NWPC [Online]. Available: http://www.elteknik.chalmers.se/Publikationer/EMKE.publ/NWPC04/papers/RUNCOS.PDF, 2004.

[4] L. Holdsworth, X. G. Wu, J. B. Ekanayake, and N. Jenkins, "Comparison of fixed speed and doubly-fed induction wind turbines during power system disturbances," *IEE Proc. Generation, Transmission and Distribution*, vol. 150, no. 3, pp. 343–352, May 2003.

[5] P. Ledesma and J. Usaola, "Effect of neglecting stator transients in doubly fed induction generators models," *IEEE Trans. Energy Conversion*, vol. 19, no. 2, pp. 459–461, Jun. 2004.

[6] S. R. Chellapilla and B. H. Chowdhury, "A dynamic model of induction generators for wind power studies," in *Proc. 2003 IEEE PES General Meeting*, vol. 4, pp. 2340–2344.

[7] J. B. Ekanayake, L. Holdsworth, X. G. Wu, and N. Jenkins, "Dynamic modeling of doubly fed induction generator wind turbines," *IEEE Trans. Power Syst.*, vol. 18, no. 2, pp. 803–809, May 2003.

[8] R. Koessler, S. Pillutla, L. Trinh, and D. Dickmander, "Integration of large wind farms into utility grids (Part 1—Modeling of DFIG)," in *Proc. 2003 IEEE PES General Meeting*, vol. 3, pp. 1511–1519.

[9] T. Thiringer, A. Petersson, and T. Petru, "Grid disturbance response of wind turbines equipped with induction generator and doubly-fed induction generator," in *Proc. 2003 IEEE PES General Meeting*, vol. 3, pp. 1542–1547.

[10] A. Tapia, G. Tapia, J. X. Ostolaza, and J. R. Sáenz, "Modeling and control of a wind turbine driven doubly fed induction generator," *IEEE Trans. Energy Convers.*, vol. 18, no. 2, pp. 194–204, Jun. 2003.

[11] S. Seman, S. Kanerva, J. Niiranen, and A. Arkkio, "Transient analysis of wind power doubly fed induction generator using coupled field circuit model," presented at the Int. Conf. ICEM 2004, Cracow, Poland, 2004.

[12] J. Niiranen, "Voltage dip ride through a doubly fed generator equipped with active crowbar," NWPC [Online]. Available: http://www.elteknik.chalmers.se/Publikationer/EMKE.publ/NWPC04/papers/NIRRANEN.PDF, Sweden, 2004.

[13] K. P. Gokhale, D. W. Krakker, and S. J. Heikkilä, "Controller for a wound rotor slip ring induction machine." [Online]. Available: http://patft.uspto.gov, May, 2004.

[14] S. Seman, J. Niiranen, S. Kanerva, and A. Arkkio, "Analysis of a 1.7 MVA doubly fed wind-power induction generator during power systems disturbances," NORPIE [Online]. Available: http://www.elkraft.ntnu.no/norpie/10956873/Final%20Papers/046%20-%20NORP-Seman.pdf, Norway, 2004.

[15] A. Arkkio, "Analysis of induction motors based on the numerical solution of the magnetic field and circuit equations." [Online]. Available: Acta Polytechnica Scandinavica Electr. Eng. Ser., No. 59 [Online]. Available: http://lib.hut.fi/Diss/198X/isbn951226076X/, Doctoral Thesis, Helsinki, Finland, 1987.

[16] S. Kanerva, S. Seman, and A. Arkkio, "Simulation of electric drive systems with coupled finite element analysis and system simulator," presented at the 10th Eur. Conf. Power Electronics and Applications, Toulouse, France, Sep. 2003.

Slavomir Seman (S'03) was born in Presov, Slovakia, in 1973. He received the M.Sc. degree in electrical engineering from University of Zilina, Slovakia, in 1997. He is currently pursuing the Ph.D. degree on transient performance study of wind-power generators at Helsinki University of Technology (HUT), Finland. He is a research scientist in Laboratory of Electromechanics at HUT.

His research interests include numerical analysis of electric machines, modeling and simulation of electric machines and control of electric drives and frequency converters.

Jouko Niiranen (M'88–SM'03) was born in 1953, in Finland. He received the M.Sc. degree in electrical engineering in 1980 and Dr. Tech. degree in electrical engineering in 1990, both from Helsinki University of Technology, Finland.

Currently he is a Senior Scientists with ABB Oy, Drives, Helsinki, Finland. He strated with Stromberg (later ABB) traction drives in 1981. During 1989 to 1993, he was as a Researcher with the Power Electronics and Electric Drives Laboratory of Helsinki University of Technology. Since 1993, he has worked with ABB in various research positions.

His main areas of research interest are modeling and simulation of electric machines, conrol of high performance drives and power electronic converters.

Dr. Niiranen is also an Adjunct Professor at Helsinki University of Technology, Finland, since 1994.

Sami Kanerva was born in Vantaa, Finland, in 1975. He received the M.Sc., Lic.SC., and D.Sc. degrees from the Helsinki, University of Technology, Finland, in 1999, 2001, and 2005, respectively.

During 1999 to 2004, he was a Research Scientist in Laboratory of Electromechanics, Helsinki University of Technology. Nowadays, he is working as an R&D engineer at ABB Oy, Machines, Helsinki, Finland. His research interests include the numerical analysis of electrical machines.

Antero Arkkio was born in Vehkalahti, Finland, in 1955. He received the M.Sc. (Tech) and D.Sc. (Tech) degrees from Helsinki University of Technology (HUT) in 1980 and 1988, respectively. He has worked with various research projects dealing with modeling, design and measurements of electrical machines.

Mr. Arkkio has been the Professor of electrical engineering (Electromechanics) at Helsinki University of Technology since 2001. Before his appointment as Professor, he has been a Senior Research Scientist and Laboratory Manager at HUT.

Julius Saitz was born in Kosice, Slovakia, in 1971. He received the M.S. degree from the University of Zilina, Zilina, Slovakia, in 1995 and the Ph.D. degree from Helsinki University of Technology in 2001. He continued to work at Helsinki University of Technology as a Reasearch Scientist and a Lecturer. In December 2004, he joined Ansoft Corporation where he currently works as an application engineer.

His research interests include numerical analysis of electric machines and other eletromechanical systems and modeling of magnetic hysteresis.